PHYSICAL REVIEW B **92**, 144413 (2015)

Electronic, magnetic, and transport properties of Fe-intercalated $2H$-TaS_2 studied by means of the KKR-CPA method

S. Mankovsky,* K. Chadova, D. Ködderitzsch, J. Minár, and H. Ebert
Department Chemie, Physikalische Chemie, Universität München, Butenandstrasse 5-13, 81377 München, Germany

W. Bensch
Institut für Anorganische Chemie, Universität Kiel, Olshausenstrasse 40, 24098 Kiel, Germany

(Received 31 July 2015; revised manuscript received 25 September 2015; published 12 October 2015)

The electronic, magnetic, and transport properties of Fe-intercalated $2H$-TaS_2 have been investigated by means of the Korringa-Kohn-Rostoker (KKR) method. The nonstoichiometry and disorder in the system have been accounted for using the coherent potential approximation (CPA) alloy theory. A pronounced influence of disorder on the spin magnetic moment has been found for the ferromagnetically ordered material. The same applies for the spin-orbit-induced orbital magnetic moment and magnetocrystalline anisotropy energy. The temperature dependence of the resistivity of disordered $2H$-$Fe_{0.28}TaS_2$ investigated on the basis of the Kubo-Středa formalism in combination with the alloy analogy model has been found in very satisfying agreement with experimental data. This also holds for the temperature-dependent anomalous Hall resistivity $\rho_{xy}(T)$. The role of thermally induced lattice vibrations and spin fluctuations for the transport properties is discussed in detail.

DOI: 10.1103/PhysRevB.92.144413 PACS number(s): 71.20.Be, 72.80.−r, 75.30.Gw

I. INTRODUCTION

Transition metal dichalcogenides are very attractive materials both from a fundamental point of view as well as concerning potential technological applications. They are formed by well separated trilayers of the type MX_2 (M: transition metal, X: S, Se, Te), that determine their quasi-2D structure leading to various interesting physical properties. These are for instance strongly anisotropic transport properties [1] or charge density wave (CDW) instabilities leading to the formation of CDW phases which can coexist at low temperature with superconductivity [2–4]. Many discussions in the literature concern the optoelectronic properties of the semiconducting dichalcogenides and their relation to the features of the energy gap such as width and direct or indirect character [5,6].

Most of the transition metal dichalcogenides are nonmagnetic. However, they allow the intercalation of magnetic atoms or molecules between the X-M-X trilayers. This leads to an interesting class of magnetic materials having quasi-2D properties [7–10] which can be varied via the amount and type of intercalated atoms. This is demonstrated in the present theoretical work on Fe-intercalated $2H$-TaS_2, where the Fe atoms occupy the octahedral holes between prismatic MX_2 trilayers (see Fig. 1). In fact, Fe-intercalated $2H$-TaS_2 can be seen as a prototype material that has been investigated experimentally already some years ago as the closely related intercalated $2H$-structured systems $NbSe_2$, $TaSe_2$, NbS_2, and TaS_2 with the magnetic $3d$ metals Mn, Fe, Co, and Ni as an intercalate [11–14]. As was shown, a common feature of these materials is the trend to create two-dimensional ordered 2×2 and $\sqrt{3} \times \sqrt{3}$ structures within the $3d$ layer for the concentration $x = 1/4$ and $1/3$, respectively, of the intercalate.

Depending on concentration and intercalation atom type, these materials exhibit for the ordered phase ferromagnetic (FM) [8] or antiferromagnetic (AFM) [11] magnetic order at low temperatures. The AFM order has been observed for the intercalated NbS_2 systems, e.g., $Fe_{1/3}NbS_2$, $Co_{1/3}NbS_2$, and $Ni_{1/3}NbS_2$, while in the case of TaS_2-based alloys intercalated by $3d$ metals FM order has been found [8] for $Cr_{1/3}TaS_2$ ($T_C = 116$ K), $Mn_{1/3}TaS_2$ ($T_C = 70$ K), and $Fe_{1/3}TaS_2$ ($T_C = 35$ K). In the case of nonstoichiometric, disordered systems the Curie temperature depends in addition on the concentration of the $3d$ element [9,10]. A strong dependence of T_C on the Fe concentration was found in particular for Fe_xTaS_2 [9] with $T_C = 90$, 163, 90, and 55 K for $x = 0.2$, 0.26, 0.28, 0.34, respectively. At $x = 0.45$ the system becomes AFM with a Néel temperature $T_N = 85$ K [10].

Ordered $Fe_{1/4}TaS_2$ possesses a very pronounced out-of-plane magnetocrystalline anisotropy (MCA); i.e., the easy axis is along the c axis. The extremely high anisotropy field B_A of about 60 T [15,16], that is by an order of magnitude higher than observed for $Mn_{1/4}TaS_2$ and $Mn_{1/4}NbS_2$ [7] (about 0.5 T), leads to an Ising-type behavior of the Fe magnetic moment.

The transport properties of magnetic intercalated transition metal dichalcogenides have been investigated by various authors. Examples for this are the electrical resistivity and anomalous Hall effect (AHE) [11] studied for alloys based on $2H$-NbS_2. The magnetotransport and superconducting properties of disordered Fe intercalation compounds based on $NbSe_2$, $TaSe_2$, and TaS_2 have been investigated by Whitney *et al.* [17] for the dilute regime ($x < 0.1$). Recently, the results of magnetotransport measurements for $Fe_{1/4}TaS_2$ have been reported by Morosan *et al.* [18]. This material shows a strong anisotropy concerning the magnetization as well as the resistivity. Checkelsky *et al.* [15] focused on the temperature dependence of the resistivity of $Fe_{1/4}TaS_2$. These authors showed that the characteristics of the AHE for $T > 50$ K cannot be explained by the Karplus-Luttinger or Berry-phase mechanism. Instead it was concluded that it is governed by scattering processes connected with temperature-induced phonons and magnons. These authors also discussed the unconventional behavior of the magnetoresistance as a function of temperature.

*Sergiy.Mankovskyy@cup.uni-muenchen.de

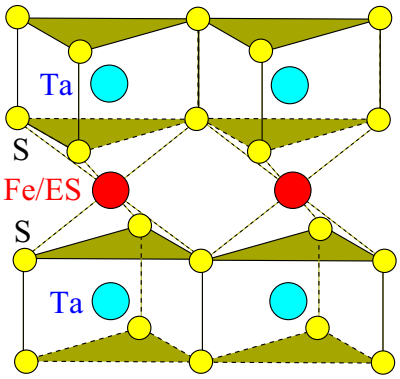

FIG. 1. (Color online) The structure of the investigated Fe-intercalated 2*H*-TaS_2 system showing the position occupied by the Fe atoms and empty spheres (ES) in between the S-Ta-S trilayers according to the Fe concentration.

A very large magnetoresistance (MR) has been found recently for disordered $Fe_{0.28}TaS_2$ single crystal by Hardy *et al.* [19], which is nearly 100 times stronger than that observed for the ordered $Fe_{1/4}TaS_2$ compound. The authors point out the crucial role of spin disorder and strong spin-orbit coupling in the system, that can be exploited to create materials with large MR.

In the present work we will focus on TaS_2 intercalated with Fe as a prototype material for magnetic intercalated transition metal dichalcogenides. While several experimental studies on the magnetic and transport properties of this system can be found in the literature, only few theoretical investigations [20,21] have been done so far with the focus on its electronic structure assuming an ordered state.

II. COMPUTATIONAL DETAILS

The present theoretical investigations on the magnetic and transport properties of Fe-intercalated 2*H*-TaS_2 are based on first-principles electronic structure calculations which have been performed using the fully relativistic Korringa-Kohn-Rostoker (KKR) Green's function method [22,23]. The combination with the coherent potential approximation (CPA) alloy theory allowed us to deal with disorder on the Fe sublattice as well as the impact of finite temperatures on transport properties on the basis of the alloy analogy model (see below). The self-consistent calculations have been done in the framework of the local approximation to spin density functional theory (LSDA) using the parametrization for the exchange and correlation potential as given by Vosko *et al.* [24]. Correlation effects going beyond the level of LSDA have been accounted for by means of the LDA+U scheme [25–27] using for Fe the parameters $U = 4.5$ eV and $J = 0.7$ eV [21] throughout. For double-counting part of the LDA+U functional the so-called atomic limit expression was used [28].

The parameters specifying the structure of Fe-intercalated 2*H*-TaS_2 as shown in Fig. 1 have been taken from experiment [10,18].

For the angular momentum expansion of the Green's function a cutoff of $l_{\max} = 3$ was applied. This is in particular important for the transport calculations that were based on the Kubo-Středa formalism [29] that among others gives access to the AHE [30]. To deal with the temperature dependence of the transport properties a scheme has been used that is based on the alloy analogy model and that accounts for thermal lattice vibrations [31] as well as spin fluctuations [32]. Within this approach the spin fluctuations are represented by a temperature-dependent quasistatic spin configuration corresponding to the adiabatic approximation [33]. The spin configuration used as an input for the transport calculations may be determined for example by performing Monte Carlo simulations or deduced from the experimental temperature-dependent magnetization [32]. Here, the latter scheme has been applied using experimental data from Ref. [19].

III. RESULTS

A. Electronic structure

At low temperatures, pure 2*H*-TaS_2 exhibits a charge density wave (CDW) instability [34] driven by the Fermi surface nesting mechanism, bringing the system into the CDW state below $T_{\mathrm{CDW}} = 80$ K [3]. Intercalation with Fe obviously strongly modifies the Fermi surface due to Fe-related electronic states resulting in a shift of the Fermi energy and a smearing of the electronic bands due to the disorder within the Fe layers. This suppresses the CDW instability and the intercalated system shows conventional metallic behavior.

These findings are reflected by the results of calculations on the electronic structure. Figure 2 shows the corresponding spin-integrated Bloch spectral function (BSF) $A(\vec{k},E)$ calculated for 2*H*-TaS_2, disordered $Fe_{0.25}TaS_2$, as well as ordered $Fe_{1/4}TaS_2$. To avoid the use of an extremely fine mesh of $\vec{k}$ and E points these calculations were done using a small imaginary part of the energy E in the case of the ordered compounds TaS_2 and $Fe_{1/4}TaS_2$. The resulting BSF for TaS_2 corresponds essentially to the dispersion relation $E(\vec{k})$ given by Blaha [35] with the differences primarily to be ascribed to the impact of the spin-orbit coupling that is accounted for within the present fully relativistic calculations. Intercalation of Fe leads for the disordered case, apart from the exchange splitting, primarily to a broadening of the bands as can be seen from Fig. 2(b). For ordered $Fe_{1/4}TaS_2$, on the other hand, the band structure gets much more complex due to the increase of the size of the unit by a factor of 4 and the occurrence of new Fe-related states [see Fig. 2(c)].

The various features in the BSF in Fig. 2 are also reflected by the component and spin-resolved density of states (DOS) shown in Fig. 3 for Fe (a), Ta (b), and S (c) in pure TaS_2, disordered $Fe_{0.25}TaS_2$, as well as ordered $Fe_{1/4}TaS_2$.

The rather broad Fe energy bands [Fig. 3(a)] indicate a significant hybridization with the electronic states of the host atoms, especially with the neighboring S atoms. This can also be concluded from the partial DOS of S, shown in Fig. 3(c). Obviously, disorder in the Fe sublattice leads for Fe itself to quite pronounced changes when compared to the ordered case; apart from a broadening and resulting smearing of the spectral features in the Fe DOS one notices a substantial redistribution of spectral weight together with an apparent change in the exchange splitting. For the S and Ta sublattices, on the other side,

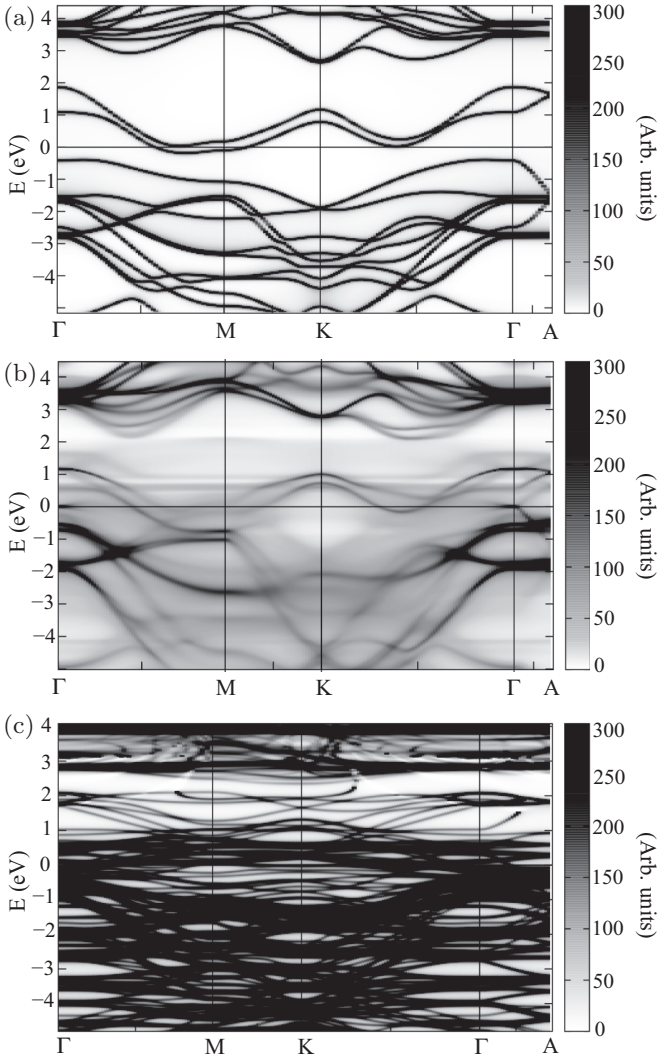

FIG. 2. Spin-integrated Bloch spectral function $A(\vec{k}, E)$ along high-symmetry directions of the Brillouin zone calculated for (a) 2*H*-TaS_2, within LSDA; (b) ferromagnetic disordered $Fe_{0.25}TaS_2$, within LSDA+*U*; and (c) ferromagnetic ordered $Fe_{1/4}TaS_2$, within LSDA+*U*. In the case of ordered compounds, TaS_2 and ordered $Fe_{1/4}TaS_2$, the BSF was calculated for a small imaginary part $\mathrm{Im}(E) = 0.001$ Ry of the energy E.

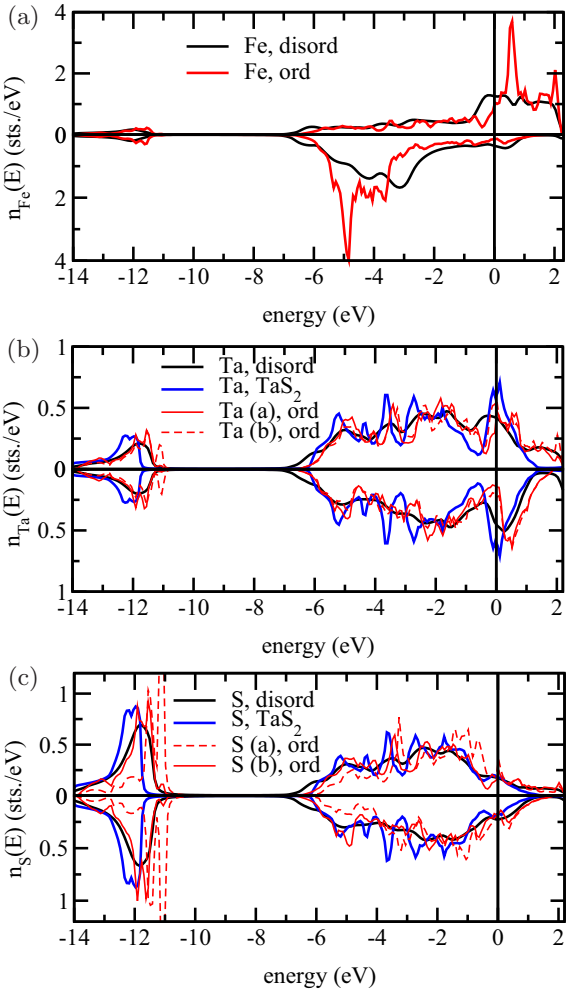

FIG. 3. (Color online) Fe (a), Ta (b), and S (c) DOS in pure TaS_2 (within LSDA) and ferromagnetic disordered $Fe_{0.25}TaS_2$ as well as ordered $Fe_{1/4}TaS_2$ (within LDA+*U*). In the cases of Ta (b) and S (c) the thin solid and dashed red lines represent the DOS for two inequivalent sites, a and b, in ordered $Fe_{1/4}TaS_2$.

disorder leads first of all to a smearing of the DOS curve. Interestingly the impact of disorder for Ta is at least as pronounced as for the S, being next-nearest neighbor to Fe (see Fig. 1).

B. Magnetic moments

Calculations of the magnetic moments for ferromagnetic disordered 2*H*-Fe_xTaS_2 have been done first using the GGA approach for the treatment of exchange and correlation. As this led to results that were too low when compared to experiment (see below) the LDA+*U* method was used instead with the corresponding parameters given in Sec. II. As can be seen from Fig. 4 this led for disordered 2*H*-Fe_xTaS_2 to a spin magnetic moment that increases nearly monotonically from about 2.42 to 3.05 μ_B when the Fe concentration x increases from 0.05 to 0.5. On the other hand, the relatively large spin-orbit-induced

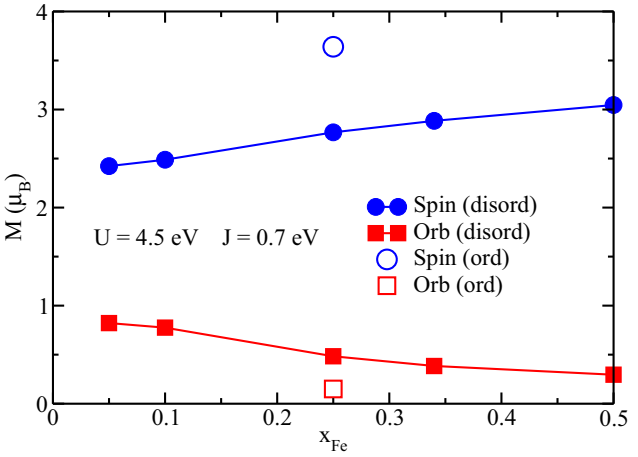

FIG. 4. (Color online) Spin (circles) and orbital (squares) magnetic moments of Fe in ferromagnetic 2*H*-Fe_xTaS_2 as a function of the Fe concentration. Results for the disordered state are given by full symbols while those for ordered 2*H*-$Fe_{1/4}TaS_2$ are given by open symbols.

orbital moment decreases from about 0.82 to 0.29 μ_B. In the case of ordered 2*H*-$Fe_{1/4}TaS_2$ quite pronounced changes compared to the disordered state are found; upon ordering the spin moment increases from 2.76 to 3.64 μ_B while the orbital moment decreases from 0.48 to 0.16 μ_B. For the GGA calculations the corresponding changes are 1.93 to 3.1 μ_B for the spin moment and 0.12 to 0.11 μ_B for the orbital moment. The increase of the spin magnetic with ordering is quite common and can often be associated with the DOS of the ordered state that is more structured and less broad than for the disordered state (see Fig. 3). For the same reason one has usually also an increase of the orbital magnetic moment. On the other hand, the orbital magnetic moment depends much more on the details of the electronic structure in the vicinity of the Fermi energy than the spin magnetic moment. This together with the relatively small width of the Fe subband seems to be the reason for the observed pronounced decrease for the orbital moment upon ordering.

The LDA+*U*-based results differ quite substantially from that of Ko *et al.* [21] who used the GGA+*U* scheme with the values for *U* and *J* as given in Sec. II and spin-orbit coupling treated as a perturbation. This approach led for the spin and orbital magnetic moment to the values 2.95 and 1.0 μ_B, respectively. These results imply that in particular the orbital magnetic moment depends quite sensitively on the treatment of exchange and correlation as well as spin-orbit coupling.

Experimental work on ordered 2*H*-$Fe_{1/4}TaS_2$ led to a total magnetic moment per Fe atom of 3.9 μ_B and a Curie temperature of $T_C = 160$ K [18]. This is in close agreement with more recent work by Checkelsky *et al.* [15] ($T_C = 160$ K) as well as Choi *et al.* [16]. The latter authors did measurements on ordered samples obtained as grown (AG) and by slow cooling (SC) leading to a total moment of 4.0 μ_B and a Curie temperature of $T_C = 156$ and 159 K, respectively. Additional measurements on quenched (Q) disordered samples led to a substantially lower Curie temperature of $T_C = 104$ K.

On the basis of XMCD measurements at the $L_{2,3}$ edges of Fe the ratio of the spin (m_{spin}) to the orbital (m_{orb}) moment has been estimated to be $m_{orb}/m_{spin} = 0.33$ [21]. Assuming an ionic configuration for Fe with a spin moment of 4.0 μ_B an orbital moment of 1.33 μ_B was suggested. Using instead the value 4.0 μ_B for the total moment as given above an orbital moment of 1.0 μ_B results from the analysis of the XMCD measurements.

When comparing the experimental results with the theoretical ones given in Fig. 4 one finds that the spin magnetic moment calculated for the 2*H*-$Fe_{1/4}TaS_2$ compound is in a good agreement with the experimental data while the orbital one seems to be too low. This might be to a large extent due to the pronounced dependence of the orbital magnetic moment on the computational details that was discussed above.

C. Magnetocrystalline anisotropy

The magnetocrystalline anisotropy energy ΔE_{MCA} defined as the difference in energy for the in-plane and out-of-plane orientation of the magnetization has been calculated by means of the so-called torque method [36]. $\Delta E_{MCA}(x)$ determined this way for disordered Fe_xTaS_2 as a function of the Fe concentration x and expressed with respect to the formula unit (see below) increases monotonically with x. To compare with experimental data $\Delta E_{MCA}(x)$ was converted into an anisotropy field $B_A = \Delta E_{MCA}/M_{f.u.}$, where the magnetic moment per formula unit ($M_{f.u.}$) is given by that per Fe atom via $M_{f.u.} = xM_{Fe}$. Using this representation for the magnetocrystalline anisotropy $B_A(x)$ decreases monotonically with x as can be seen in Fig. 5. For $x = 0.25$ calculations have been done in addition assuming an ordered compound $Fe_{1/4}TaS_2$. As often found, ordering increases the anisotropy field in a quite pronounced way. Astonishingly, this consequence of ordering for $\Delta E_{MCA}(x)$ is reversed when compared to the situation for the orbital magnetic moment. Comparison of the theoretical result for B_A with the experimental value for $x = 1/4$ confirms the large anisotropy field found in experiment. Nevertheless, the theoretical value for the ordered as well as for the disordered state is well above the experimental value. This indicates again that a certain amount of disorder may be present in the sample investigated. Another reason for the deviation between theory and experiment might be the treatment of electronic correlations. The comparison of magnetic moments calculated on the basis of plain LDA with experiment clearly demonstrates that one has to go beyond that scheme (see above). While this is obviously also true in the case of the magnetocrystalline anisotropy [21], the numerical results depend to some extent on the details of the adopted computational scheme. The LDA+*U* method with the values for *U* and *J* as given above leads obviously in a coherent way to reasonable results for the magnetic moment as well as magnetocrystalline anisotropy when compared to experiment. This also applies for the transport properties to be discussed below.

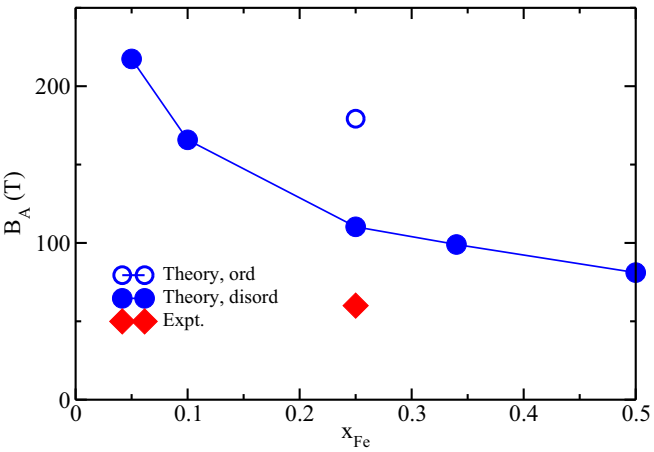

FIG. 5. (Color online) Magnetocrystalline anisotropy in the Fe-intercalated TaS_2 vs Fe concentration. The diamond represents the MCA energy measured at 2 K [15,16] (anisotropy field $B_A = 60$ T).

D. Electrical resistivity

The temperature-dependent longitudinal electrical resistivities, $\rho_{xx}(T) = \rho_{yy}(T)$ and $\rho_{zz}(T)$, calculated for ferromagnetic disordered 2*H*-$Fe_{0.28}TaS_2$ using the scheme described in Sec. II are shown in Fig. 6(a). For the in-plane longitudinal electrical resistivity $\rho_{xx}(T)$ results are given in addition that account

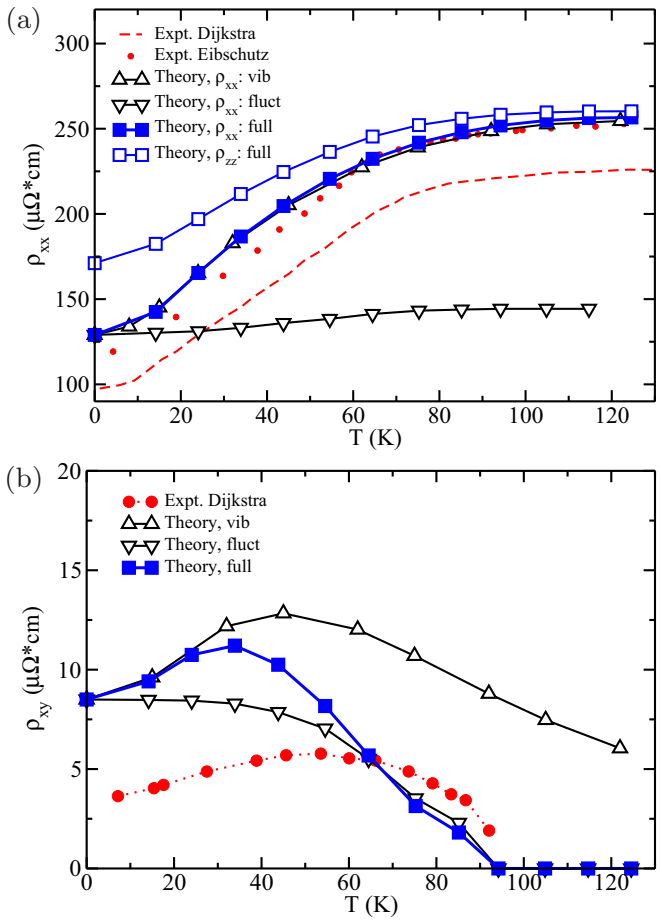

FIG. 6. (Color online) (a) Temperature-dependent longitudinal resistivities, $\rho_{xx}(T) = \rho_{yy}(T)$ and $\rho_{zz}(T)$ (filled and open squares), for ferromagnetic disordered 2*H*-$Fe_{0.28}TaS_2$. The dots [9] and the dashed line [20] represent corresponding experimental data. (b) Temperature-dependent transverse resistivity, $\rho_{xy}(T)$. Results for $\rho_{xx}(T)$ and $\rho_{xy}(T)$ that were obtained accounting only for lattice vibrations and spin fluctuations are represented in both cases by up and down triangles, respectively.

only for the lattice vibrations (vib) and spin fluctuations (fluct). For $T = 0$ K all individual $\rho_{xx}(T)$ curves represent the residual resistivity due to the random disorder in the Fe sublattice. Keeping the magnetic spin configuration fixed and dealing only with the impact of thermal lattice vibrations on the resistivity a pronounced and monotonic increase with temperature is observed for the corresponding curve $\rho_{xx}^{vib}(T)$ (up triangles). Considering on the other hand $\rho_{xx}^{fluct}(T)$ (down triangles) that accounts for the spin fluctuations only one finds a rather weak increase with temperature. Accounting for both temperature-dependent scattering mechanisms simultaneously one finds for the resulting curve $\rho_{xx}(T)$ (full squares) only minor changes compared to $\rho_{xx}^{vib}(T)$. As found before for ferromagnetic bcc-Fe [32], this finding clearly shows that $\rho_{xx}^{fluct}(T)$ and $\rho_{xx}^{vib}(T)$ are not additive; i.e., the Matthiesen rule is violated. Comparing the calculated $\rho_{xx}(T)$ curve with the available experimental data [9,20] one can see that the experimental and theoretical residual resistivities agree rather well. The fact that the theoretical values are somewhat higher may indicate that the assumption of fully random disorder on the Fe sublattice for the calculations is not fully justified; i.e., there might be some order present in the experimentally investigated samples. In fact, for both experimental works [9,20] referred to above, superstructure reflections have been observed by x-ray diffraction indicating a relatively high degree of order. This explains that the residual resistivity is somewhat lower in experiment than in theory. Furthermore, as pointed out by Dijkstra *et al.* [20], the scatter among the experimental data is caused not only by the degree of order but in addition by the degree of stoichiometry. Keeping these influencing factors on the experimental resistivity in mind, agreement between theory and experiment is quite satisfying. In particular one has to note that the theory as well as all experimental curves agree very well concerning the temperature dependence.

The various curves in Fig. 6(a) clearly show that the thermal lattice vibrations are primarily responsible for the temperature dependence of $\rho_{xx}(T)$ including the change of its slope close to the Curie temperature. For that reason this peculiar behavior cannot be ascribed to the temperature-induced magnetic disorder as was assumed before [9,20]. Obviously, the temperature dependence of $\rho_{xx}(T)$ has primarily to be ascribed to the increasing smearing of the energy bands with temperature due to electron scattering caused by lattice vibrations. For low temperature, this results in a rather fast increase of the resistivity due to a corresponding increasing cross section for the interband scattering. For higher temperatures, a saturation of the number of channels for the interband scattering seems to occur leading finally to a rather weak increase of $\rho_{xx}(T)$ with temperature.

As can be seen in Fig. 6(a), the calculated out-of-plane resistivity $\rho_{zz}(T)$ for $T = 0$ K is larger than its in-plane counterpart $\rho_{xx}(T)$ reflecting the 2D-character of the system. The finding that this difference is relatively weak is due to the disorder in the Fe sublattice that causes in both cases a large residual resistivity. With increasing temperature this difference diminishes monotonically being nearly absent for the highest temperature considered here ($T = 125$ K). This behavior of the resistivity has been observed and discussed before for example for the compounds Nb_3Sn and Nb_3Sb [37–39]. The fact that the $\rho_{zz}(T)$ curve is not shifted rigidly against that for $\rho_{xx}(T)$ clearly shows once more that the contributions to the resistivity due to chemical and thermal disorder are not simply additive. This nonadditive behavior together with the fact that the temperature dependence for $\rho_{xx}(T)$ as well as for $\rho_{zz}(T)$ is obviously dominated by the thermal lattice vibrations leads obviously to the decreasing anisotropy of the resistivity with increasing temperature seen in Fig. 6(a).

The temperature-dependent transverse electrical resistivity $\rho_{xy}(T)$ for disordered 2*H*-Fe_xTaS_2 is shown in Fig. 6(b). For $T = 0$ K the various theoretical curves are determined only by the chemical disorder on the Fe sub-lattice and for that reason all coincide. The value $\rho_{xy}(0)$ may be decomposed into its intrinsic or coherent and extrinsic or incoherent contribution [30,40]. The later part represents in particular all so-called skew scattering contributions. Keeping the spin configuration fixed to that for $T = 0$ K (corresponding to a collinear ferromagnetic ordering) and accounting for the lattice vibrations only the resulting $\rho_{xy}^{vib}(T)$ rises with temperature T and shows a broad maximum around 40 K. For higher

temperatures $\rho_{xy}^{vib}(T)$ decreases with T as was found before for example in the case of pure Ni in the regime below the Curie temperature [31]. On the other hand, if the lattice structure is kept undistorted and spin fluctuations are accounted for $\rho_{xy}^{fluct}(T)$ monotonically decreases with T until the Curie temperature is reached and $\rho_{xy}^{fluct}(T)$ vanishes as the thermally averaged z component of the magnetization $\langle M_z \rangle_T$ vanishes. If both scattering mechanisms are accounted for one finds again that these do not act in a simple additive way. Nevertheless, from the behavior of the individual curves $\rho_{xy}^{vib}(T)$ and $\rho_{xy}^{fluct}(T)$ one may expect the behavior of the transverse resistivity $\rho_{xy}(T)$ that accounts for the lattice vibrations and spin fluctuations simultaneously. When comparing these results with the corresponding experimental data, a reasonable agreement is found, in particular concerning the presence of a maximum for $\rho_{xy}(T)$ with temperature. The individual curves $\rho_{xy}^{vib}(T)$ and $\rho_{xy}^{fluct}(T)$ clearly demonstrate the importance of extrinsic contributions to $\rho_{xy}(T)$ supporting the conclusions of Checkelsky *et al.* [15] concerning their role for Fe_xTaS_2 mentioned in the introduction.

IV. SUMMARY

Using the KKR-CPA band structure method for disordered systems the electronic structure as well as magnetic and transport properties of ferromagnetic ordered and disordered $2H$-Fe_xTaS_2 have been investigated. By means of the fully relativistic KKR-CPA the spin-orbit-induced orbital magnetic moment and magnetocrystalline anisotropy energy could be calculated in particular. The various magnetic properties were found in reasonable agreement with available experimental data with clear indications for the strong impact of the degree of order on the Fe sublattice of the system. In addition, a prominent role of correlation effects was found that was ascribed to relatively narrow width of the Fe-related bands. The temperature dependence of the longitudinal resistivity as well as transverse anomalous Hall resistivity was studied using the alloy analogy model within the framework of the Kubo-Středa formalism. The results obtained for disordered $2H$-$Fe_{0.28}TaS_2$ were found in very satisfying agreement with experimental data. Additional calculations accounting for thermally induced lattice vibrations and spin fluctuations individually clearly showed that their contribution to the resistivity is not additive and that the temperature dependence of the longitudinal resistivity is nearly exclusively determined by the lattice vibrations.

ACKNOWLEDGMENTS

Financial support by the Deutsche Forschungsgemeinschaft (DFG) via the priority programs SPP 1415 and SPP 1538 is thankfully acknowledged.

[1] R. Friend and A. Yoffe, Adv. Phys. **36**, 1 (1987).
[2] J. Wilson, F. D. Salvo, and S. Mahajan, Adv. Phys. **24**, 117 (1975).
[3] R. L. Withers and J. A. Wilson, J. Phys. C: Solid State Phys. **19**, 4809 (1986).
[4] A. H. Castro Neto, Phys. Rev. Lett. **86**, 4382 (2001).
[5] J. Wilson and A. Yoffe, Adv. Phys. **18**, 193 (1969).
[6] Q. H. Wang, K. Kalantar-Zadeh, A. Kis, J. N. Coleman, and M. S. Strano, Nat. Nanotechnol. **7**, 699 (2012).
[7] S. S. P. Parkin and R. H. Friend, Philos. Mag. B **41**, 65 (1980).
[8] S. S. P. Parkin and R. H. Friend, Philos. Mag. B **41**, 95 (1980).
[9] M. Eibschütz, S. Mahajan, F. J. DiSalvo, G. W. Hull, and J. V. Waszczak, J. Appl. Phys. **52**, 2098 (1981).
[10] H. Narita, H. Ikuta, H. Hinode, T. Uchida, T. Ohtani, and M. Wakihara, J. Solid State Chem. **108**, 148 (1994).
[11] R. H. Friend, A. R. Beal, and A. D. Yoffe, Philos. Mag. **35**, 1269 (1977).
[12] J. van den Berg and P. Cossee, Inorg. Chim. Acta **2**, 143 (1968).
[13] K. Anzenhofer, J. V. D. Berg, P. Cossee, and J. Helle, J. Phys. Chem. Solids **31**, 1057 (1970).
[14] B. V. Laar, H. Rietveld, and D. Ijdo, J. Solid State Chem. **3**, 154 (1971).
[15] J. G. Checkelsky, M. Lee, E. Morosan, R. J. Cava, and N. P. Ong, Phys. Rev. B **77**, 014433 (2008).
[16] Y. J. Choi, S. B. Kim, T. Asada, S. Park, W. Wu, Y. Horibe, and S-W. Cheong, Europhys. Lett. **86**, 37012 (2009).
[17] D. A. Whitney, R. M. Fleming, and R. V. Coleman, Phys. Rev. B **15**, 3405 (1977).
[18] E. Morosan, H. W. Zandbergen, L. Li, M. Lee, J. G. Checkelsky, M. Heinrich, T. Siegrist, N. P. Ong, and R. J. Cava, Phys. Rev. B **75**, 104401 (2007).
[19] W. J. Hardy, C.-W. Chen, A. Marcinkova, H. Ji, J. Sinova, D. Natelson, and E. Morosan, Phys. Rev. B **91**, 054426 (2015).
[20] J. Dijkstra, P. J. Zijlema, C. F. van Bruggen, C. Haas, and R. A. de Groot, J. Phys.: Condens. Matter **1**, 6363 (1989).
[21] K.-T. Ko, K. Kim, S. B. Kim, H.-D. Kim, J.-Y. Kim, B. I. Min, J.-H. Park, F.-H. Chang, H.-J. Lin, A. Tanaka, and S.-W. Cheong, Phys. Rev. Lett. **107**, 247201 (2011).
[22] H. Ebert *et al.*, Munich SPR-KKR Package, Version 6.3, http://olymp.cup.uni-muenchen.de/ak/ebert/SPRKKR.
[23] H. Ebert, D. Ködderitzsch, and J. Minár, Rep. Prog. Phys. **74**, 096501 (2011).
[24] S. H. Vosko, L. Wilk, and M. Nusair, Can. J. Phys. **58**, 1200 (1980).
[25] A. B. Shick, A. I. Liechtenstein, and W. E. Pickett, Phys. Rev. B **60**, 10763 (1999).
[26] A. N. Yaresko, V. N. Antonov, and P. Fulde, Phys. Rev. B **67**, 155103 (2003).
[27] H. Ebert, A. Perlov, and S. Mankovsky, Solid State Commun. **127**, 443 (2003).
[28] M. T. Czyżyk and G. A. Sawatzky, Phys. Rev. B **49**, 14211 (1994).
[29] L. Smrčka and P. Středa, J. Phys. C: Solid State Phys. **10**, 2153 (1977).
[30] S. Lowitzer, D. Ködderitzsch, and H. Ebert, Phys. Rev. Lett. **105**, 266604 (2010).

[31] D. Ködderitzsch, K. Chadova, J. Minár, and H. Ebert, New J. Phys. **15**, 053009 (2013).
[32] H. Ebert, S. Mankovsky, K. Chadova, S. Polesya, J. Minár, and D. Ködderitzsch, Phys. Rev. B **91**, 165132 (2015).
[33] V. P. Antropov, M. I. Katsnelson, B. N. Harmon, M. van Schilfgaarde, and D. Kusnezov, Phys. Rev. B **54**, 1019 (1996).
[34] I. Guillamón, H. Suderow, J. G. Rodrigo, S. Vieira, P. Rodière, L. Cario, E. Navarro-Moratalla, C. Martí-Gastaldo, and E. Coronado, New J. Phys. **13**, 103020 (2011).
[35] P. Blaha, J. Phys.: Condens. Matter **3**, 9381 (1991).
[36] J. B. Staunton, L. Szunyogh, A. Buruzs, B. L. Gyorffy, S. Ostanin, and L. Udvardi, Phys. Rev. B **74**, 144411 (2006).
[37] R. W. Cohen, G. D. Cody, and J. J. Halloran, Phys. Rev. Lett. **19**, 840 (1967).
[38] Z. Fisk and G. W. Webb, Phys. Rev. Lett. **36**, 1084 (1976).
[39] P. B. Allen and B. Chakraborty, Phys. Rev. B **23**, 4815 (1981).
[40] I. Turek, J. Kudrnovský, and V. Drchal, Phys. Rev. B **86**, 014405 (2012).